International Journal of
Georesources and Environment
http://ijge.camdemia.ca, ijge@camdemia.ca
IJGE 2017 **3**(**3**): 73-84
Available at http://ojs.library.dal.ca/ijge
Section – Geohazards and Environment

Estimation of Quality Factor (Q_β) Using Accelerograms of Ahar-Varzaghan Earthquakes, Northwestern Iran

Majid Mahood*, Saman Amiri
Earthquake Prediction Center, International Institute of Earthquake Engineering and Seismology, Tehran, Iran

Abstract: High-frequency strong-motion data of two recent major earthquakes in the Ahar-Varzaghan region, Northwestern Iran, have been used to determine shear-wave quality factor ($Q_\beta(f)$) and seismic source parameters. Data from a local array of 12 stations, two main shocks (Ahar-Varzaghan doublet earthquakes (M_w 6.4 and 6.3) on August 11, 2012), and 38 aftershocks of magnitude 4.1 – 5 were analyzed. The classic Brune model is used to predict the shape of the source spectrum and to provide scaling relationships between spectral and source parameters. In order to obtain reliable estimates of the source spectrum, the effects of attenuation need to be estimated and corrected. By using an inversion algorithm in this work, an average relation in the form $Q_\beta = (114 \pm 21) f^{(0.90 \pm 0.07)}$ is obtained. The best fit theoretical spectrum provides final values of source parameters, i.e. seismic moment M_o and corner frequency f_c as 3.19×10^{25} dyne cm and 0.69 Hz, respectively, for the first event. Obtained $Q(f)$ relationship suggests a low Q_o value (< 200) and a high n value (> 0.8) for high heterogeneous, tectonically and seismically active regions.

Keywords: Attenuation, $Q_\beta(f)$, Inversion, Ahar-Varzaghan Earthquake, NW-Iran

1 Introduction

Frequency-dependent seismic wave attenuation strongly depends on the physical conditions of the underground crustal media. Attenuation is a petrophysical parameter that is sensitive to lithology and physical properties such as pressure, temperature, saturation with fluid, gas, etc. (Toksöz et al 1979). The value of attenuation in the crust, commonly described by a dimensionless quantity known as quality factor Q shows a close relation with seismic activity. This parameter is used to measure the tendency of material to dissipate energy during deformations. The common idea is being considered Q as a ratio of potential energy to dissipated energy over one period of harmonic deformations (Sato et al 2012). Changes in Q value with time may be attributed to an increase of pressure in the crust producing new cracks and/or reopening of pre-existing cracks, which are the most viable mechanisms for increasing attenuation (Mahood 2014).

The source spectrum has important information of earthquake source and wave propagation medium, therefore is directly employed to compute various source parameters like stress drop, seismic moment, corner frequency and source radius. Simulation of strong-motion is made with these parameters by using different simulation techniques such as empirical Green function and stochastic simulation techniques (Hartzell 1978, Hanks and McGuire 1981, Boore 1983). Analysis of source spectrum provides important information, which is used in strong ground motion prediction.

Recently, a technique has been developed by Joshi (2006a) which uses the *S*-phase of an accelerogram as input in an inversion algorithm and gives $Q_\beta(f)$ and corner frequency f_c of the input events. The approach suggested by Joshi (2006a) and subsequently modified by Joshi et al (2012) was applied to calculate the $Q_\beta(f)$ and source parameters. The greatest advantage of this method is its accuracy and rapidness. Kumar et al (2015) studied shear wave attenuation by using a modified inversion of strong-motion data in the Kumaon Himalaya, India. Some studies of source, path, and site characteristics were conducted by: Sharma et al (2014) for the Uttarakhand Himalaya region using accelerogram data from 15 earthquakes, Joshi et al (2014) for the Sikkim region of India after an earthquake of M_w 6.9 occurred on September 18, 2011, and He et al (2015) and Joshi et al (2016) after the April 25, 2015, M_w 7.9 Nepal earthquake.

Several researchers have used different techniques to determine seismic attenuation in different regions in Iran. For the East-Central Iran, Mahood and Hamzehloo (2009, 2011) and Mahood et al (2009) estimated the coda wave attenuation and high frequency *P*- and *S*-waves attenuation, respectively. Motaghi and Ghods (2012) studied the attenuation of ground-motion spectral amplitudes and its variations across the central Alborz Mountains. Rahimi et al (2010) and Farrokhi et al (2015) estimated coda-wave attenuation in the central and eastern Alborz. Farrokhi and Hamzehloo (2016) investigated body wave attenuation

* Corresponding Author: Majid Mahood, Email: m.mahood@iiees.ac.ir

DOI: 10.15273/ijge.2017.03.008

characteristics in the Alborz region and north central Iran. In the NW Iran, however, much less work has been conducted. Among of those, Zafarani et al (2015) found the frequency-dependent *S*-wave quality factor, $Q_s = 99\ f^{0.77}$, from the stochastic simulation of strong-motion records of the Ahar-Varzaghan earthquakes.

This article uses data from the strong-motion network installed in the NW Iran to study the seismicity and attenuation of shear waves in this region. We have used the vertical component of acceleration records, which is supposedly free from the site effects. Forty events recorded at 12 stations are utilized in the present work. The input parameters, such as seismic moment and corner frequency, are calculated from an inversion algorithm.

2 Methodology

2.1 Study region and data

The 6.4 M_w Ahar-Varzaghan (named after two nearby cities) earthquake occurred at 12:23 UTC on August 11, 2012, in East Azerbaijan province in northwestern Iran (Fig. 1). It was followed 11 min later by a second shock at 6.3 M_w. The comparable magnitudes of the two events and their close spatial and temporal relationship justify them as an earthquake doublet (Xu and Schwartz 1993). The doublet mainshocks were followed by three events of magnitude 5+ and many smaller aftershocks. The seismicity affected both Varzaghan and Ahar and seriously, damaged about 20 villages, killed 327 people and injured more than 3000 (Razzaghi and Ghafory-Ashtiany 2012).

The region of NW Iran is exceptional within the Arabian-Eurasian continental collision zone. The tectonics is dominated by the NW-SE striking right-lateral North Tabriz Fault (NTF), which is a major seismogenic fault in this region. Historical seismicity in the northwest of Iran is mostly associated with this Fault (Fig. 1). NW Iran is a region of intense deformation and seismicity situated between two thrust belts of the Caucasus to the north and the Zagros Mountains to the south (Hessami et al 2003). Earthquake focal mechanisms suggest that the convergence

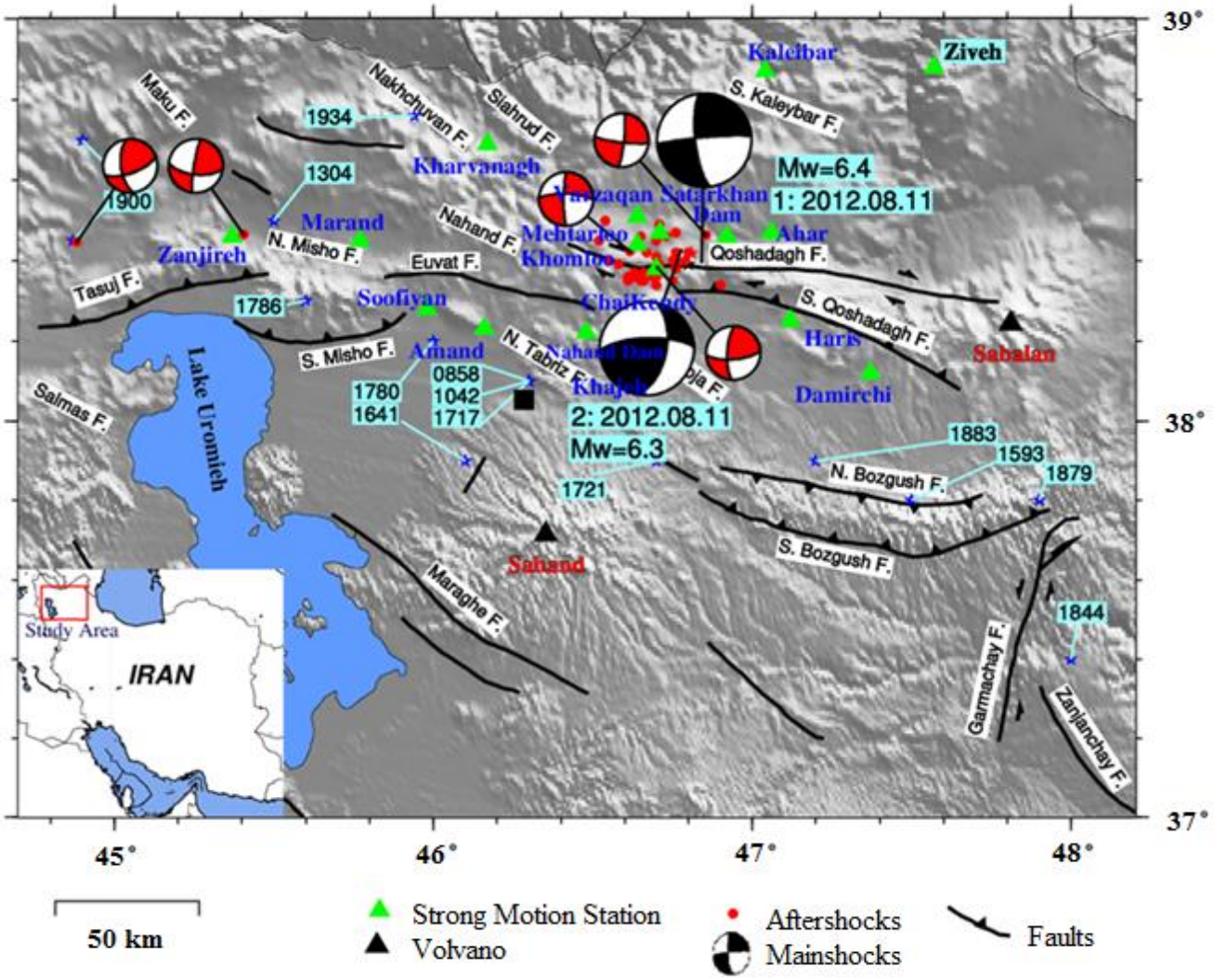

Figure 1. An overview of topography and historical events (by date) of NW Iran with the Ahar-Varzeghan earthquakes and aftershocks (red circle), mechanisms for both mainshocks and five aftershoks, strong-motion stations (green triangles) and active faults.

between Arabia and Eurasia has been accommodated mainly through WNW-trending right-lateral strike-slip faults in this region. These strike-slip faults appear to be the southeastern continuation into NW Iran of the North Anatolian Fault and other right-lateral faults in SE Turkey (Jackson 1992). From paleoseismological observations conducted in several trenches cutting the fault at different places, Hessami et al (2003) and Solaymani-Azad et al (2011) concluded that the NTF experienced at least three strong earthquakes since 33.5 ka (Fig. 1). Last sequence of three events during the 18th century ruptured the total length of the NTF, and since that time, no large earthquake has been located on this fault (Moradi et al 2011). The Ahar-Varzaghan doublet occurred in a region characterized as having a low deformation rate and being bounded by deep-seated faults, among which the NTF is capable to trigger a destructive earthquake (Hessami et al 2003, Donner et al 2015, Ghods et al 2015).

Figure 1 shows an overview of northwestern Iran with topography, destructive and historical events (defined by date), location of the Ahar-Varzeghan earthquakes, focal mechanisms for both mainshocks and five aftershoks according to international agencies (e.g. Harvard Centroid Moment Tensor), strong-motion stations and active faults. The last damaging earthquakes on NTF occurred in 1721, rupturing the southeastern fault segment, and in 1780, rupturing the northwestern section. Tabriz, one of the major cities in NW Iran, suffered major damage in both 1721 and 1780 events.

The doublet mainshocks and various aftershocks used in the present study were recorded at different stations from August 11 to November 7, 2012. Locations of the mainshocks and 38 aftershoks used for Q_β estimation are shown in Fig. 1. The strong ground motion network, installed by the Building and Housing Research Centre since 1972, includes 12 stations. All instruments were composed of SSA-2 digital accelerographs with a 10-Gal (0.1 m/s^2) threshold, sampling rate of 200 Hz, and natural frequency of 50 Hz.

These earthquakes were recorded in more than 50 strong-motion stations but we considered 40 accelerograms that have relatively strong signal to noise ratios (S/N > 3) which enabled a relatively accurate determination of the source parameters and *Q* factor. The magnitudes of the aftershoks are from 4.1 to 5.5 and were recorded at distances of less than 100 km from the hypocenter. For separating *S*-wave window of each record, the *S*-wave time window is determined by Kinoshita (1994) method.

To analyze the acceleration records, in the first step, all recorded waveforms were corrected for drift and baseline by following the algorithm developed by Boore and Bommer (2005). In the second step, waveforms were low-pass filtered, with cutoff frequency at 25 Hz, and then vectorized and a time window containing the direct *S*-wave was selected from the accelerograms by using the Kinoshita (1994) algorithm. The displacement amplitude spectrum of each acceleration record, at each recording station, was computed by applying Fast Fourier Transform (FFT) to the corresponding time window, and the output of the Fourier transform was post-multiplied by ω^2 to obtain displacement spectrum (Figs. 2 & 3).

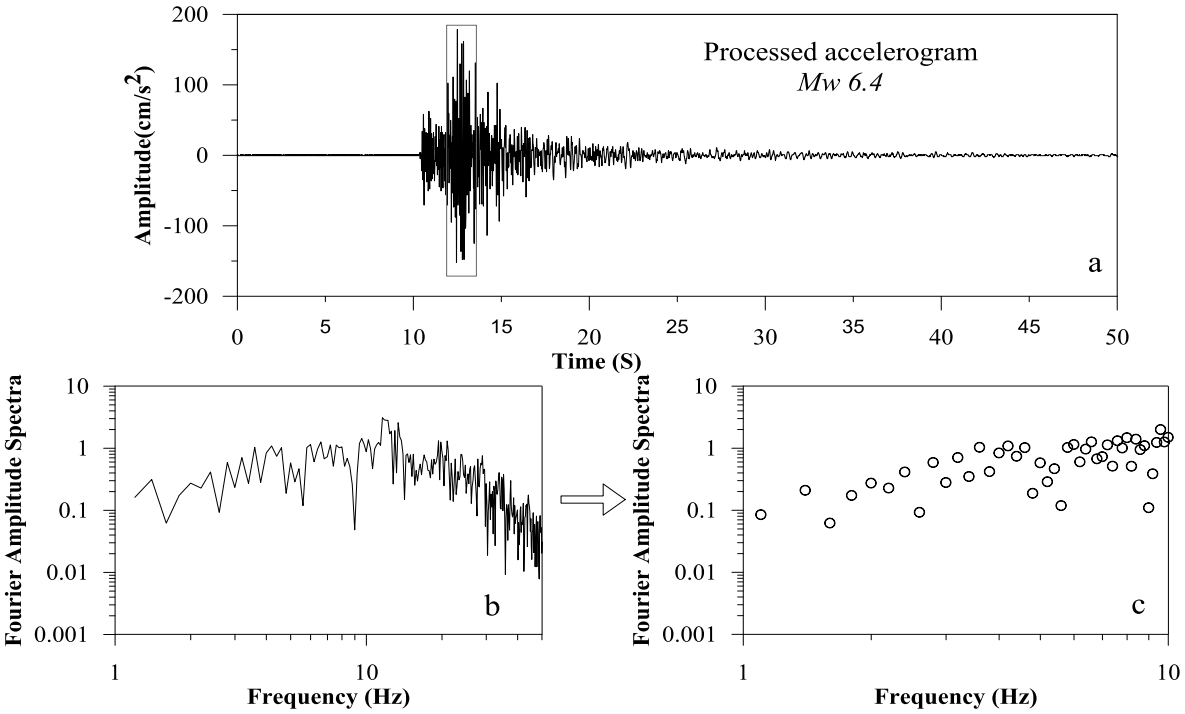

Figure 2. (a) Processed accelerogram at AHAR station; (b) Acceleration spectrum of *S*-phase marked by rectangular block with a time window of 4.0 s; (c) Discrete values of acceleration spectra used for present inversion (the discrete values of acceleration spectra are shown by small circles).

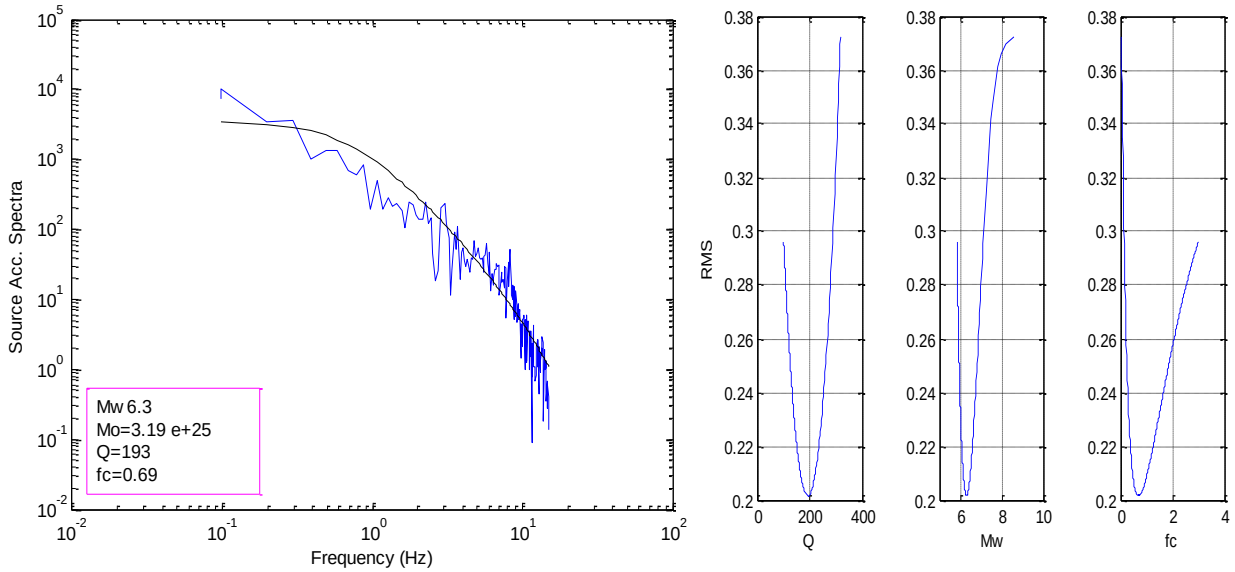

Figure 3. Left: the observed spectra and the fitted Brune source model. Right: the error values between theoretical and observed models for Q_β, M_w and f_c parameters.

2.2 Inversion

In this article we applied an inversion scheme for obtaining frequency-dependent $Q_\beta(f)$. We used least-squares inversion method for a singular value decomposition technique for a singular matrix (Joshi 2006a).

Seismic moment is one of the most important parameters, which is required as an input to the present algorithm. This is computed from the source spectrum of the recorded data by using Brune's model (Brune 1970). In this process, a time window of length covering the entire *S*-phase is applied to the corrected accelerogram. The sampled window is cosine tapered with 10% taper at both ends (Sharma and Wason 1994). The spectrum of this time series is obtained by using a FFT algorithm and is then corrected for the anelastic attenuation and geometrical spreading terms. The plots of median source spectra of the events, as computed from the recorded data, are shown in Figs 3 & 4. By using the long-term flat levels in these spectra, the seismic moment of each event is calculated. Based on Brune's model, the seismic moment M_o of an earthquake can be calculated from the long-term flat level of the displacement spectrum given by:

$$M_o = \frac{4\pi\rho\beta^3\Omega_o R}{R_{\theta\varphi}} \quad (1)$$

where ρ and β is the density and *S*-wave velocity of the medium, respectively, Ω_o is the long-term flat level of the source displacement spectrum at the hypocentral distance R, and $R_{\theta\varphi}$ is the radiation pattern coefficient. We use the density of medium as 2.8 g/cm^3 and shear wave velocity as 3.5 km/s (Zafarani et al 2015), respectively. The fault plane solution for each event used in the present work could not be determined owing to the small number of recording stations. Therefore, the radiation pattern term $R_{\theta\varphi}$ for *S*-wave is approximately taken as 0.55 (Atkinson and Boore 1995). To estimate the moment magnitude using relation of Hanks and Kanamori (1979):

$$M_W = \frac{2}{3} log(M_0) - 10.7 \quad (2)$$

The acceleration spectrum of shear waves at distance R due to an earthquake of seismic moment M_o can be given at frequency f as (Boore 1983, Atkinson and Boore 1998):

$$A(f) = CS(f, f_c)D(f) \quad (3)$$

where the term C is constant at a particular station for a given earthquake, $S(f, f_c)$ represents the source acceleration spectrum, and $D(f)$ denotes a frequency-dependent diminution function that takes into account the anelastic attenuation and attenuation due to geometrical spreading. This function modifies the spectral shape and is given as (Boore and Atkinson 1987):

$$D(f) = [e^{(-\pi f R/Q(f)\beta)}\mathrm{G(R)}]\ \mathrm{P}(f, f_m) \quad (4)$$

where $P(f, f_m)$ is a high-cut filter and $e^{(-\pi fR/Q(f)\beta)}G(R)$ is a propagation filter. $P(f, f_m)$ takes into account the fact that above some cutoff frequency (f_m), acceleration spectra show a sharp decrease (Boore 1983). In the present work, we have observed that above 25 Hz, the acceleration spectra decrease rapidly. Therefore, f_m is considered as 25 Hz in the analytical form of $P(f, f_m)$ given by Boore (1983). The term $e^{(-\pi fR/Q(f)\beta)}$ represents anelastic attenuation. In this term, $Q(f)$ is the frequency-dependent shear-wave quality factor, which needs to be determined. The function $G(R)$ represents the geometrical spreading term and is assumed to be equal to $1/R$ for $R < 100$ km and equal to $1/(10R^{0.5})$ for $R > 100$ km (Singh et al 2006). As we are using the data from those events, which lie at the hypocentral distances ≤ 100 km, $G(R)$ is assumed as $1/R$. The geometrical factor term has been used as $1/R$ for the strong-motion studies of

worldwide earthquakes by Boore (1983), Atkinson and Boore (1995), Joshi and Midorikawa (2004), Joshi (2006b) and Kumar et al (2015).

For a double-couple seismic source embedded in an elastic medium, on considering only *S*-waves, *C* is a constant for a given station for a particular earthquake and is given as (Boore 1983):

$$C = M_o\, R_{\theta\varphi}.\ FS.\ PRTITN/(4\pi\rho\beta^3) \qquad (5)$$

in which M_o is the seismic moment, $R_{\theta\phi}$ is the radiation pattern, *FS* is the amplification due to the free surface, *PRTITN* is the reduction factor that accounts for partitioning of energy into two horizontal components, and ρ and β are the density and the shear-wave velocity, respectively. In the inversion procedure, the vertical component of a record is used to remove the possibility of site effects in the horizontal components. Therefore, in order to have consistency in the inversion procedure, source spectra are computed from the vertical components of records. For computing seismic moments in the inversion procedure from the vertical components, we do not include the term, which accounts for the division of energy into two horizontal components. It is also noticed that corner frequencies for the vertical and horizontal motions will not be the same. In order to keep consistency in the approach we compute source parameters from the vertical components and same components are used for inversion.

The $S(f, f_c)$ in Equation (3) defines the source spectrum of the earthquake. On using the spectral shape based on the ω^{-2} decay of high frequency proposed by Aki and Chouet (1975) and Brune (1970), $S(f, f_c)$is defined as:

$$S(f, f_c) = (2\pi f)^2/(1 + (f/f_c)^2) \qquad (6)$$

Equation (3) serves as a foundation for the inversion algorithm. It should be linearized to determine the unknown parameter. Therefore, Equation (3) is linearized by taking its natural logarithm as follows:

$$\ln A(f) = \ln C + \ln\left(S(f, f_c)\right) - \pi f R/Q_\beta(f)\beta \qquad (7)$$
$$? \ln(R) + \ln P(f\ \ f_m)$$

where $Q_\beta(f)$ and f_c are unknown. The term representing the source spectrum $S(f, f_c)$ can be replaced with Equation (5). Further, with the assumption that f_c is known, the unknown parameter, $Q_\beta(f)$, can be obtained from the inversion by minimizing it in a least-squares sense. The least-squares inversion minimizes:

$$\chi^2 = \sum[A_s(f) - S(f, f_c)]^2 \qquad (8)$$

where $S(f, f_c)$ is the theoretical source-acceleration spectrum and $A_s(f)$ is the source spectrum obtained from the record after substituting parameters $Q_\beta(f)$ obtained from the inversion. Rearranging the known and unknown quantities on different sides of Equation (6) and substituting the term related to the source spectrum $S(f, f_c)$ as $(2\pi f)^2/(1+(f/f_c)^2)$, we obtain the following form:

$$-\pi f R/Q_\beta(f)\beta = \ln A(f) - \ln C - \ln(2\pi f)^2 \qquad (9)$$
$$+\ln[1+(f/f_c)^2] + \ln(R) - \ln P(f, f_m)$$

In Equation (9), the dependence on the corner frequency was linearized by expanding $\ln(1+(f/f_c)^2)$ in a Taylor series around f_c. Accordingly, the following expression was obtained:

$$-\pi f R/Q_\beta(f)\beta = \ln A(f) - \ln C$$
$$-\ln[(2\pi f)^2/(1+(f/f_c)^2)]$$
$$-[2/(1+(f/f_c)^2)](f/f_c)^2(\Delta f_c/f_c) \qquad (10)$$
$$+\ln(R) - \ln P(f, f_m)$$

where Δf_c is the small change in the corner frequency and is an unknown quantity that is obtained from the inversion. In Equation (10), the fourth term on the right side represents the Taylor series expansion of a fourth term in Equation (9) as given by Fletcher (1995) and Joshi (2006a).

We obtained the following set of equations at a particular station for the *i*th earthquake for frequencies f_1, f_2, f_3, …, f_n, where *n* denotes the total number of digitized samples in the acceleration record:

$$-\pi f_1 R_{11}/Q_\beta(f_1)\beta + F(f_1/f_{c1})\Delta f_c = D_{11}(f_1)$$
$$-\pi f_2 R_{11}/Q_\beta(f_2)\beta + F(f_2/f_{c1})\Delta f_c = D_{11}(f_2) \qquad (11)$$
$$\ldots$$
$$-\pi f_n R_{11}/Q_\beta(f_n)\beta + F(f_n/f_{c1})\Delta f_c = D_{11}(f_n)$$

where $F(f_1, f_c)=[2/(1+(f_1/f_c)^2)](f_1/f_c)^2(1/f_c)$ is the term obtained from the expansion of $\ln(1+(f/f_c)^2)$ in terms of a Taylor series around f_c. This function behaves linearly for known values of corner frequency f_c. For this reason, in the present work, f_c was used as an input parameter; its several possibilities were checked, and its final value was selected by minimizing the root mean square error (RMSE). For another station, the set of equations is

$$-\pi f_1 R_{12}/Q_\beta(f_1)\beta + F(f_1/f_{c1})\Delta f_c = D_{12}(f_1)$$
$$-\pi f_2 R_{12}/Q_\beta(f_2)\beta + F(f_2/f_{c1})\Delta f_c = D_{12}(f_2) \qquad (12)$$
$$\ldots$$
$$-\pi f_n R_{12}/Q_\beta(f_n)\beta + F(f_n/f_{c1})\Delta f_c = D_{12}(f_n)$$

Subscripts *i* and *j* represent the event and the station number, respectively. Therefore, to generalize Equation (12), $D_{ij}(f_i)$ is given as

$$D_{ij}(f_i) = \ln A_{ij}(f_{ij}) - \ln C_i$$
$$-\ln[(2\pi f)^2/(1+f/f_{ci})^2)] + \ln(R_{ij}) \qquad (13)$$
$$-\ln P(f, f_m)$$

In the matrix form, this set of equations can be written as follows:

$$
\begin{vmatrix}
(-\pi f_1 R_{11})/\beta & 0 & 0 & \cdots & 0 & F(f_1,f_{c1}) & 1/Q_\beta(f_1) & D_{11}(f_1) \\
0 & (-\pi f_2 R_{11})/\beta & 0 & \cdots & 0 & F(f_2,f_{c1}) & 1/Q_\beta(f_2) & D_{11}(f_2) \\
0 & 0 & (-\pi f_3 R_{11})/\beta & \cdots & 0 & F(f_3,f_{c1}) & 1/Q_\beta(f_3) & D_{11}(f_3) \\
\vdots & \vdots & \vdots & & \vdots & \vdots & \vdots & \vdots \\
0 & 0 & 0 & \cdots & (-\pi f_n R_{11})/\beta & F(f_n,f_{c1}) & \vdots & D_{11}(f_n) \\
(-\pi f_1 R_{12})/\beta & 0 & 0 & \cdots & 0 & F(f_1,f_{c1}) & \vdots & D_{12}(f_1) \\
0 & (-\pi f_2 R_{12})/\beta & 0 & \cdots & 0 & F(f_2,f_{c1}) & \vdots & D_{12}(f_2) \\
0 & 0 & (-\pi f_3 R_{12})/\beta & \cdots & 0 & F(f_3,f_{c1}) & \vdots & D_{12}(f_3) \\
\vdots & \vdots & \vdots & & \vdots & \vdots & \vdots & \vdots \\
0 & 0 & 0 & \cdots & (-\pi f_n R_{12})/\beta & F(f_n,f_{c1}) & \vdots & D_{12}(f_n) \\
 & & & & & & \vdots & \vdots \\
 & & & \textit{for mth earthquake} & & & \vdots & \vdots \\
(-\pi f_1 R_{m1})/\beta & 0 & 0 & \cdots & 0 & F(f_1,f_{cm}) & \vdots & D_{m1}(f_1) \\
0 & (-\pi f_2 R_{m1})/\beta & 0 & \cdots & 0 & F(f_2,f_{cm}) & \vdots & D_{m1}(f_2) \\
0 & 0 & (-\pi f_3 R_{m1})/\beta & \cdots & 0 & F(f_3,f_{cm}) & \vdots & D_{m1}(f_3) \\
\vdots & \vdots & \vdots & & \vdots & \vdots & \vdots & \vdots \\
0 & 0 & 0 & \cdots & (-\pi f_n R_{m1})/\beta & F(f_n,f_{cm}) & \vdots & D_{m1}(f_n) \\
(-\pi f_1 R_{m2})/\beta & 0 & 0 & \cdots & 0 & F(f_1,f_{cm}) & \vdots & D_{m2}(f_1) \\
0 & (-\pi f_2 R_{m2})/\beta & 0 & \cdots & 0 & F(f_2,f_{cm}) & \vdots & D_{m2}(f_2) \\
0 & 0 & (-\pi f_3 R_{m2})/\beta & \cdots & 0 & F(f_3,f_{cm}) & \vdots & D_{m2}(f_3) \\
\vdots & \vdots & \vdots & \cdots & \vdots & \vdots & \vdots & \vdots \\
\vdots & \vdots & \vdots & \cdots & \vdots & \vdots & \vdots & \vdots \\
\vdots & \vdots & \vdots & \cdots & \vdots & \vdots & 1/Q_\beta(f_n) & D_{m2}(f_n) \\
0 & 0 & 0 & \cdots & (-\pi f_n R_{m2})/\beta & F(f_n,f_{cm}) & \Delta f_c &
\end{vmatrix}
$$

This matrix can be represented in the following form:

$$Gm = d \tag{14}$$

Model parameters are contained in the model matrix *m* and the spectral component in the data matrix *d*. Inversion of the *G* matrix using Newton's method gives the model matrix m as

$$m = (G^T G)^{-1} G^T d \tag{15}$$

The inversion resulting in Equation (15) is prone to problems if G^TG is even close to singular, and in such a case, singular value decomposition is used to solve Equation (15) (Press et al 1992).

The corner frequency is treated as the input parameter in the inversion algorithm to maintain the linearity in Equation (13). We have used the solution that is obtained corresponding to minimum RMSE. In the present inversion scheme, several possibilities of corner frequencies are checked by iteratively changing the corner frequency f_c in an increment of Δf. The small increment Δf considered in the present work is 0.2 Hz.

The software code required for this inversion has been developed in MATLAB for the present study. The process of obtaining spectral amplitudes from the processed time series is shown in Fig. 2, which shows processed accelerogram at AHAR station, acceleration spectrum of *S*-phase marked by rectangular block and discrete value of acceleration spectra used for present inversion.

3 Results and Discussion

We present the quality factor and seismic source characterization. Construction of the attenuation and seismic source models includes new and updated data, data types, source models and source parameters that reflect the current state of knowledge of earthquake occurrence and state of practice for seismic hazard analyses in the study region. We review the SSC parameterization and describe

the methods used to estimate earthquake rates, magnitudes, locations and geometries for all seismic source models, with an emphasis on new source model components.

For the NW Iran, less researches have been done to estimate *Q*. This is mainly because of the unavailability of sufficient data required for such work. In this research, source and path parameters are determined by using strong-motion data for 40 earthquakes recorded at the 12 stations in the study region. The advantage of using strong-motion data for the inversion is that it includes valuable high-frequency near-field data suitable for engineering use. The spectral parameters (M_o, f_c and Q_β) are estimated from the Brune's spectra after obtaining the best fit between the observed and Brune's spectra, and the measure of best fit is represented in terms of minimizing errors in a least-squares sense. The seismic moment of each event was determined using the source displacement spectra. Computed values of seismic moment at different stations were used to calculate the average seismic moment for each event. The RMS in the obtained and observed data was calculated for each case, and the solution corresponding to minimum RMS gave a direct estimate of $Q_\beta(f)$ together with the value of the corner frequency and seismic moment.

Figure 3 shows the observed spectra and a solid line which indicates the theoretical spectra of the Brune source model (left hand) for mainshock (M_w *6.4*) and the error values between theoretical and observed models for Q_β, M_w and f_c parameters (right hand). These parameters are estimated as Q_β = 193, M_w 6.3 and f_c = 0.69 Hz with minimum errors.

It is difficult to check which estimate of *Q* better describes the actual attenuation because there is no means of comparison directly or indirectly in earlier studies (Joshi 2006a). This method has an advantage that the obtained *Q*(*f*) values are checked by computing source spectra from the digital record at each station. The fit of observed spectra with a theoretical spectrum estimates the efficacy of our approach and reliability of the obtained *Q*(*f*) relationship. A numerical experiment is performed in which the *S*-phase time window has been changed and its correlation with RMS is observed for deriving the *Q*(*f*) relationship. It is seen that the selection of window in this approach is dependent on the *S*-phase present in the record. The minimum time window for the *S*-phase is 4 s in the case of data recorded at Varzaghan and Tabriz stations for the mainshocks. Minimum error is obtained for the case of 4.0 s time window and that it increases when this window is either increased or decreased. This may be due to the overlapping of other phases in the input record for larger time windows and incomplete *S*-phases in smaller time windows (Joshi et al 2010). Figure 4 shows an example of selected portions of the shear wave (4 s) and the source spectra of the first Ahar-Varzaghan earthquake (M_w *6.4*), as used for the inversion, and comparisons of the source spectra from the actual records and those from the Brune's model in three different stations; Soofian, Tabriz and Haris, respectively. Magnitudes are estimated as M_w *6.0*, *6.3*, *6.3* and Q_β = 103, 90 and 81 with minimum errors.

The average *Q(f)* relation of form $Q_o f^n$ obtained by using average Q_β values based on inversion of records at Varzaghan, Tabriz, Ziveh and Zanjireh stations are shown in Fig. 5. The average values of the $Q_\beta(f)$ for region stations are given in Table 1. The iterative inversion was performed at each station independently. Figure 5 shows that the Q_β estimates vary for near and far stations from the mainshock epicenter. Lower Q_β values can be observed for near mainshock epicenter stations (i.e. Varzaghan, Q_o = 46) and higher Q_β values for distant stations (i.e. Zanjireh, Q_o = 157). The environment of the epicenter is more affected by the released energy and seismic waves recorded in the near field are propagated in the filled crack area.

Table 1. The average values of the $Q_\beta(f)$ for region stations

Station	*Q(f)* Relation
Tabriz	$Q(f) = (92 \pm 13)\, f^{(0.76 \pm 0.09)}$
Chai Kendy	$Q(f) = (49 \pm 12)\, f^{(0.85 \pm 0.09)}$
Varzaqan	$Q(f) = (46 \pm 11)\, f^{(0.79 \pm 0.08)}$
Khajeh	$Q(f) = (77 \pm 19)\, f^{(0.78 \pm 0.07)}$
Khomloo	$Q(f) = (112 \pm 19)\, f^{(0.81 \pm 0.06)}$
Amand	$Q(f) = (96 \pm 21)\, f^{(0.82 \pm 0.07)}$
Kaleibar	$Q(f) = (52 \pm 16)\, f^{(0.92 \pm 0.08)}$
Soofiyan	$Q(f) = (110 \pm 21)\, f^{(0.74 \pm 0.08)}$
Damirchi	$Q(f) = (73 \pm 13)\, f^{(0.90 \pm 0.09)}$
Kharvanagh	$Q(f) = (140 \pm 19)\, f^{(0.69 \pm 0.09)}$
Ziveh	$Q(f) = (126 \pm 18)\, f^{(0.76 \pm 0.06)}$
Zanjireh	$Q(f) = (157 \pm 24)\, f^{(0.79 \pm 0.09)}$

The plot of average *Q(f)* values versus frequency is shown in Fig. 6. To calculate regional *Q(f)* relation, the Q_β values at each frequency obtained from inversion is averaged at different stations and is plotted in Fig. 6a. The best fit line gives $Q(f) = (114 \pm 12)\, f^{(0.9 \pm 0.07)}$, which represents regional attenuation characteristics of NW Iran. The deviation of Q_o and *n* with respect to their mean values is shown in Fig. 6b & c, respectively. The shaded area in Fig. 6b & c denotes the region deviates from mean to standard deviation, i.e. between μ+δ and μ-δ. It is seen that the calculated value of Q_o for shear wave attenuation varies between 114±12 and *n* varies between 0.9±0.07, indicating a highly heterogeneous and tectonically active region.

A comparison of $Q_\beta(f)$ obtained from present study is made with the measurements of $Q_\beta(f)$ in other parts of the world in Fig. 7. Measured Q_β values in the NW Iran are in the range of seismically active regions such as Kumaon Hymalaya (Joshi et al 2010). Figure 7 suggests that the NW Iran falls in the seismotectonically active region. As Sharma et al (2008) have noted, the area has a considerably thick layer of sediments due to which most of the energy gets dissipated into the medium.

4 Conclusion

In the present study, an inversion algorithm was performed to obtain the $Q_\beta(f)$ relationship and source parameters in the Ahar-Varzaghan region, NW Iran, using strong-motion data. The minimum error is obtained in the inversion scheme for a relationship which gives $Q_\beta = (114 \pm 21)f^{(0.90 \pm 0.07)}$ for the study region, which represents the large heterogeneities and high level of tectonic activity in this region. The estimated relation indicates high attenuating crust beneath the source region, which makes this region seismically hazardous for future earthquakes, that requires special attention to determine its seismic hazards. The obtained $Q_\beta(f)$ is used to correct the spectrum and this corrected spectrum is further utilized to compute other two parameters, i.e. seismic moment and corner frequency. The best fit Brune's (1970) theoretical spectrum with the observed corrected spectrum provides these source parameters for the earthquakes of magnitude range 4.1 to 5.5 used in present work. The obtained values M_o and f_c are 3.19×10^{25} dyne.cm and 0.69 Hz, respectively, for the Ahar-Varzaghan first earthquake.

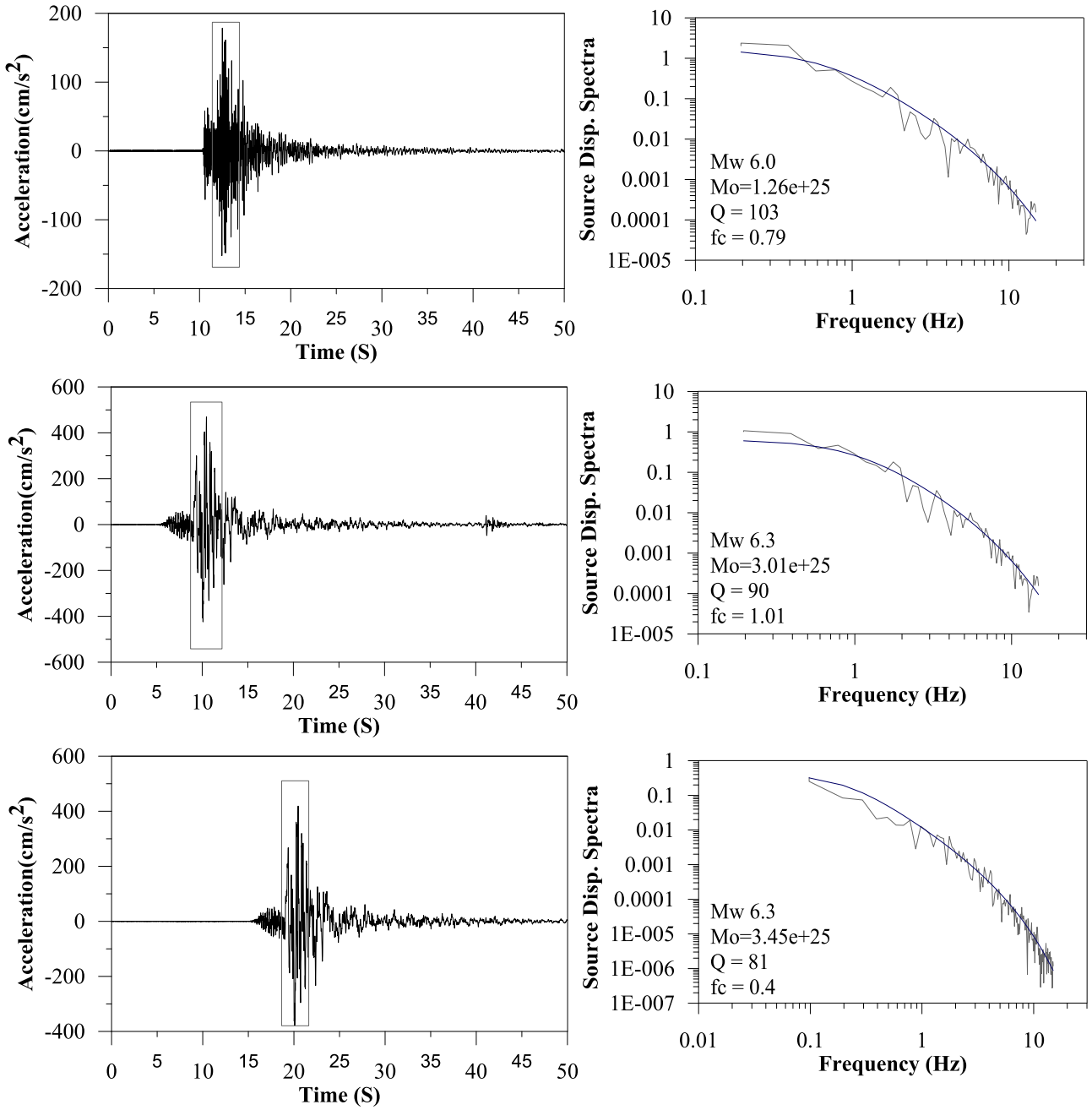

Figure 4. Selected portions of the vertical component of the accelerograms of the Ahar-Varzaghan earthquake, as used for the inversion, and comparisons of the source spectra from the actual records and those from the Brune's model (see the acceleration records at left hand in the Soofian, Tabriz and Haris stations, and the source spectra at the right hand); the thick solid line shows the theoretical Brune's spectrum, and the spectrum from the observed record is shown by the thin dark line.

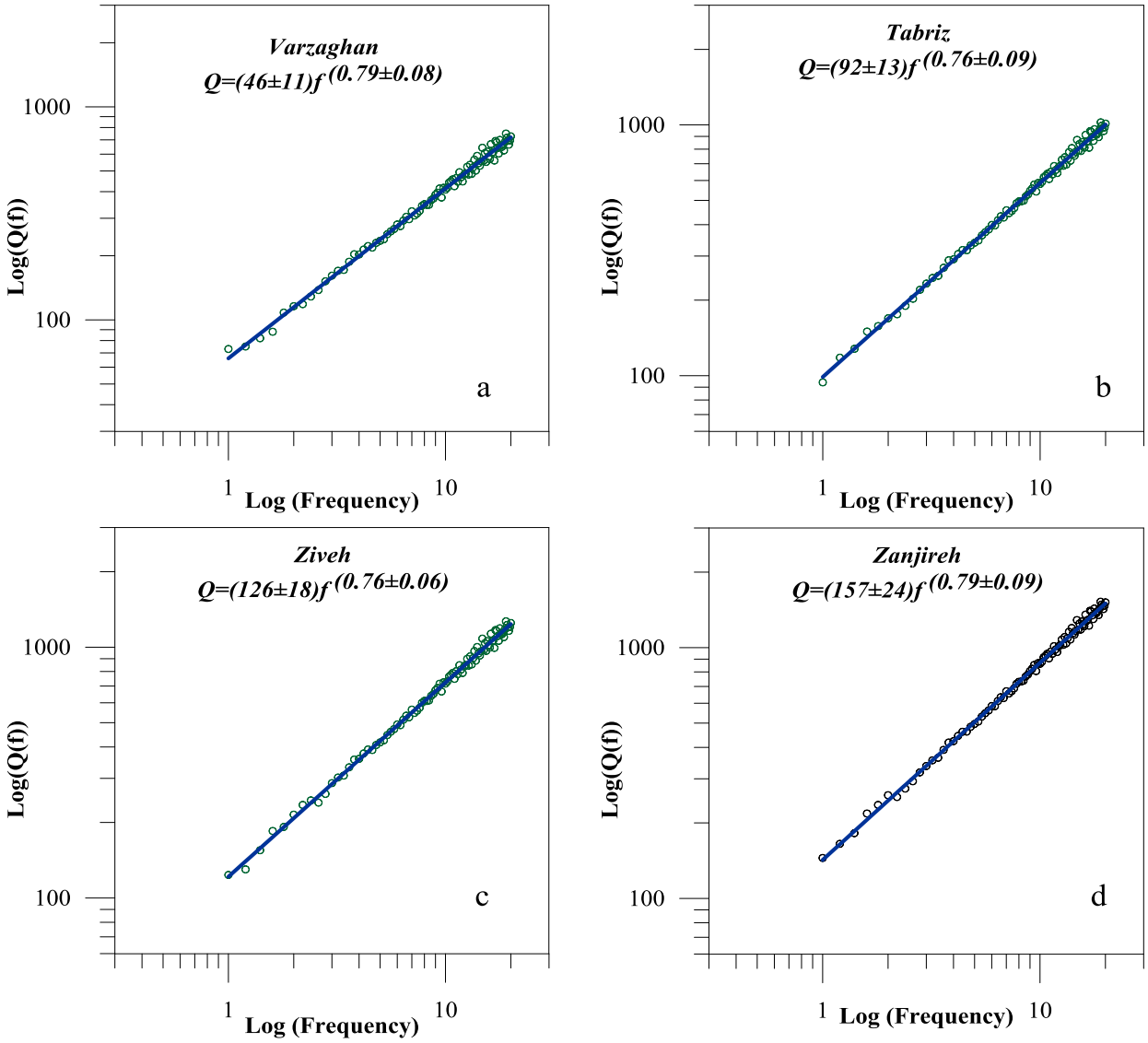

Figure 5. Obtained *Q(f)* relationship at Varzaghan (a), Tabriz (b), Ziveh (c) and Zanjireh (d) stations, respectively. The average *Q(f)* at different frequencies is taken from the value obtained after inversion of shear waves.

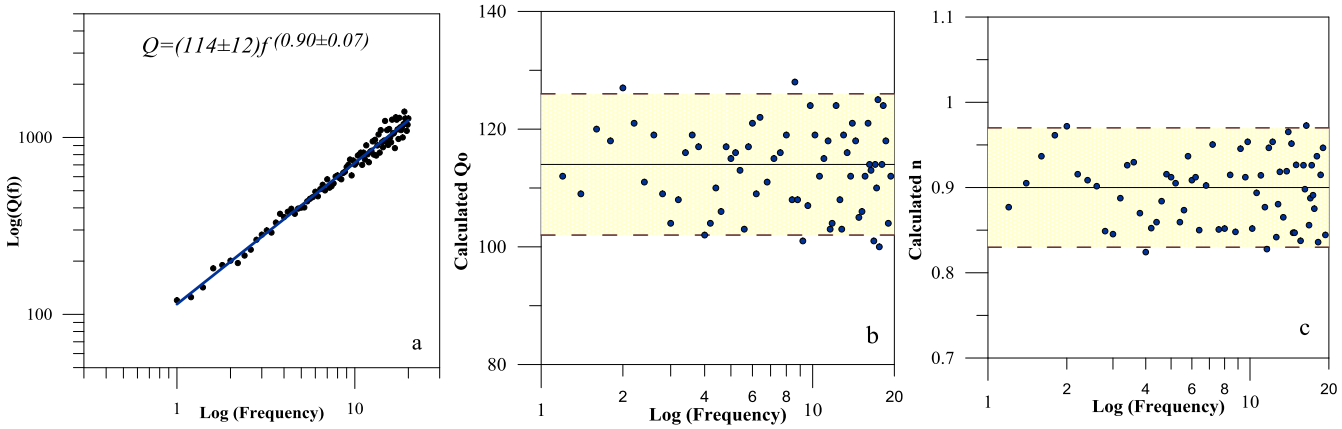

Figure 6. a) Regional $Q_\beta(f)$ relationship for NW Iran based on the obtained value of shear wave attenuation at different stations at different frequencies. b) Variation of Q_o with respect to its mean value. c) Variation of *n* with respect to its mean value. The shaded area denotes the region between μ+δ and μ-δ.

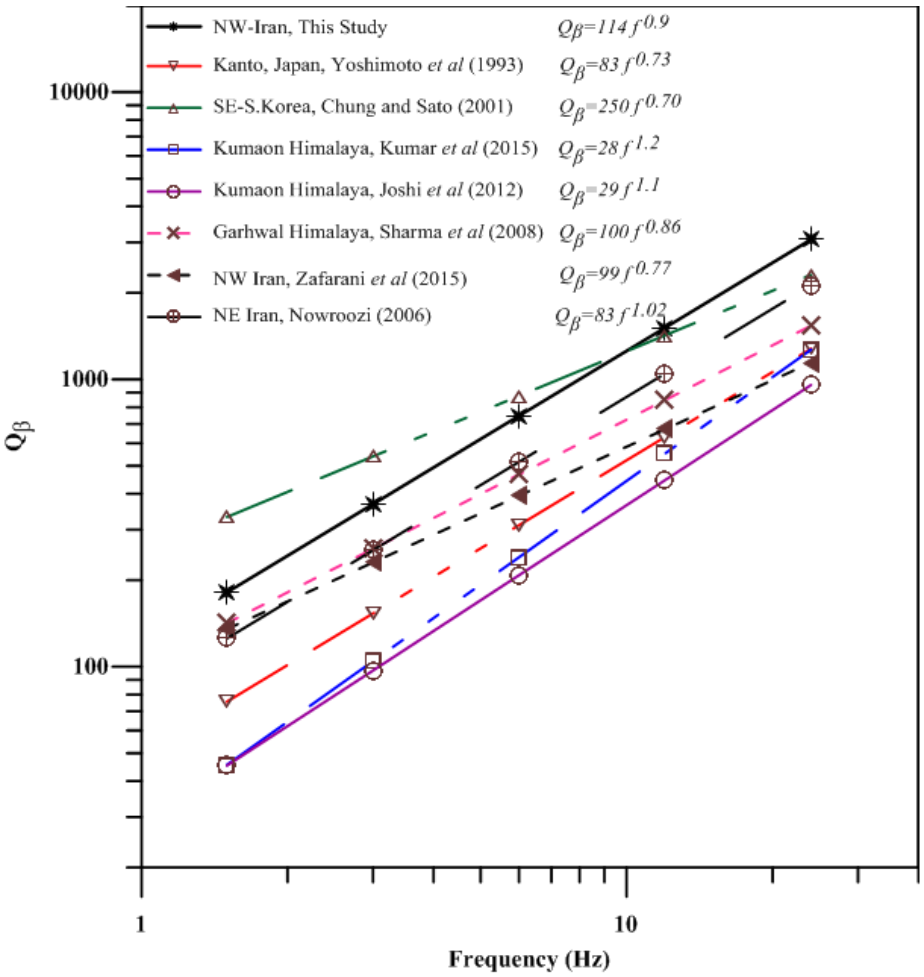

Figure 7. Comparison of $Q_\beta(f)$ relations developed in the present study with that obtained for worldwide region.

Acknowledgements

The authors sincerely thank the International Institute of Earthquake Engineering and Seismology (IIEES) for supporting this research and providing the data. The authors also want to acknowledge the Building and Housing Research Center (BHRC) of Iran for providing the data. The authors wish to thank anonymous reviewers whose suggestions help significantly in improving the paper.

References

Aki, K. and B. Chouet, 1975. Origin of coda waves: source, attenuation and scattering effects. J. Geophys. Res., **80**: 3322 - 3342.

Atkinson, G.M. and D.M. Boore, 1995. Ground-motion relation for eastern North America. Bull. Seismol. Soc. Am., **85**: 17 - 30.

Atkinson, G.M. and D.M. Boore, 1998. Evaluation of models for earthquake source spectra in eastern North America. Bull. Seism. Soc. Am., **88**: 917 - 934.

Boore, D.M., 1983. Stochastic simulation of high-frequency ground motions based on seismological models of the radiated spectra. Bull. Seism. Soc. Am., **73**: 1865 - 1894.

Boore, D.M. and G.M. Atkinson, 1987. Stochastic prediction of ground motion and spectral response parameters at hard-rock sites in eastern North America. Bull. Seism. Soc. Am., **77**: 440 - 467.

Boore, D.M. and J.J. Bommer, 2005. Processing of strong-motion accelerograms: needs, options and consequences. Soil Dynamics and Earthquake Engineering, **25**: 93 - 115.

Brune, J.M., 1970. Tectonic stress and spectra of seismic shear waves from earthquakes. J. Geophys. Res., **75**: 4997 - 5009.

Donner, S., A. Ghods, F. Krüger, D. Robler, A. Landgraf and P. Ballato, 2015. The Ahar-Varzaghan Earthquake Doublet (Mw6.4 and 6.2) of 11 August 2012: regional seismic moment tensors. Bull Seismol. Soc. Am., **105**(**2A**): 791 - 807.

Farrokhi, M., H. Hamzehloo, H. Rahimi and M. Allamehadeh, 2015. Estimation of coda-wave attenuation in the central and eastern Alborz, Iran. Bull. Seismol. Soc. Am., **105**: 1756 - 1767.

Farrokhi, M. and H. Hamzehloo, 2016. Body wave attenuation characteristics in the crust of Alborz region and North Central Iran. J. Seismol., **21**: 631 - 646.

Fletcher, J.B., 1995. Source parameters and crustal Q for

four earthquakes in South Carolina. Seism. Res. Lett., **66**: 44 - 58.

Ghods, A., E. Shabanian, E. Bergman, M. Faridi, S. Donner, G. Mortezanejad and A. Aziz-Zanjani, 2015. The Varzaghan–Ahar, Iran, Earthquake Doublet (*M*w 6.4, 6.2): implications for the geodynamics of northwest Iran. Geophys. J. Int., **203**: 522 - 540.

Hanks, T.C. and H. Kanamori, 1979. A moment magnitude scale. J. Geophys. Res., **84**: 2348 - 2350.

Hanks, T.C. and R.K. McGuire, 1981. The character of high frequency ground motion. Bull Seismol. Soc. Am., **71**: 2071 - 2095.

Hartzell, S.H., 1978. Earthquake aftershocks as Green's functions. Geophys. Research Lett., **5**: 1 - 4.

He, X., S. Ni, L. Ye, T. Lay, Q. Liu and K.D. Koper, 2015. Rapid seismological quantification of source parameters of the 25 April 2015 Nepal Earthquake. Seismol. Research Lett., **86**: 1568 - 1576.

Hessami, K., F. Jamali and H. Tabassi, 2003. Major Active Faults of Iran (map). Ministry of Science, Research and Technology, International Institute of Earthquake Engineering and Seismology.

Jackson, J., 1992. Partitioning of strike-slip and convergent motion between Eurasia and Arabia in eastern Turkey and the Caucasus. J. geophys. Res., **97**: 12 471 - 12 479.

Joshi, A., 2006a. Use of acceleration spectra for determining the frequency dependent attenuation coefficient and source parameters. Bull. Seismol. Soc. Am., **96**: 2165 - 2180.

Joshi, A., 2006b. Analysis of strong motion data of the Uttarkashi earthquake of 20th October 1991 and the Chamoli earthquake of 28th March 1999 for determining the mid crustal Q value and source parameters. J. Earthq. Technol., **43**: 11 - 29.

Joshi, A. and S. Midorikawa, 2004. A simplified method for simulation of strong ground motion using rupture model of the earthquake source. Journal of Seismology, **8**: 467 - 484.

Joshi, A., M. Mohanty, A.R. Bansal, V.P. Dimri and R.K. Chadha, 2010. Use of spectral acceleration data for determination of three dimensional attenuation structure in the Pithoragarh region of Kumaon Himalaya. J Seismol., **14**: 247 - 272.

Joshi, A., P. Kumar, M. Mohanty, A.R. Bansal, V.P. Dimri and R.K. Chadha, 2012. Determination of $Q_\beta(f)$ at different places of Kumaon Himalaya from the inversion of spectral acceleration data. Pure Appl. Geophys., **169**: 1821 - 1845.

Joshi, A., P. Kumar and S. Arora, 2014. Use of site amplification and anelastic attenuation for the determination of source parameters of the Sikkim earthquake of September 18, 2011, using far-field strong-motion data. Nat Hazards., **70**: 217 - 235.

Joshi, A., M. Tomer, S. Lal, S. Chopra, S. Singh, S. Prajapati and M.L. Sharma, 2016. Estimation of the source parameters of the Nepal earthquake from strong motion data. Nat Hazards., **83**: 867 - 883.

Kinoshita, S., 1994. Frequency-dependent attenuation of shear waves in the crust of the southern Kanto area, Japan. Bull. seism. Soc. Am., **84**: 1387 - 1396.

Kumar, P., A. Joshi, A. Sandeep, A. Kumar and R.K. Chadha, 2015. Detailed attenuation study of shear waves in the Kumaon Himalaya, India, using the inversion of strong-motion data. Bull. Seismol. Soc. Am., **105**: 836 - 1851.

Mahood, M. and H. Hamzehloo, 2009. Estimation of coda wave attenuation in east central Iran. J. Seismol., **13**: 125 - 139.

Mahood, M., H. Hamzehloo and G.J. Doloei, 2009. Attenuation of high frequency *P* and *S* waves in the crust of the East-Central Iran. Geophys. J. Int., **179**: 1669 - 1678.

Mahood, M. and H. Hamzehloo, 2011. Variation of intrinsic and scattering attenuation of seismic waves with depth in the Bam region, East-Central Iran. Soil Dynamics and Earthquake Engineering, **31**: 1338 - 1346.

Mahood, M., 2014. Attenuation of high-frequency seismic waves in Eastern Iran. Pure Appl. Geophys., **171**: 2225 - 2240.

Moradi, S., D. Hatzfeld and M. Tatar, 2011. Microseismicity and seismotectonics of the North Tabriz Fault (Iran). Tectonophysics, **506**: 22 - 30.

Motaghi, K. and A. Ghods, 2012. Attenuation of ground-motion spectral amplitudes and its variations across the central Alborz Mountains. Bull. Seismol. Soc. Am., **102**: 1417 - 1428.

Press, W.H., S.A. Teukolsky, W.T. Vetterling and B.P. Flannery, 1992. Numerical Recipes. Cambridge University Press, New York, U.S.A.

Rahimi, H., K. Motaghi, S. Mukhopadhyay and H. Hamzehloo, 2010. Variation of coda wave attenuation in the Alborz region and central Iran. Geophys. J. Int., **181**: 1643 - 1654.

Razzaghi, M.S. and M. Ghafory-Ashtiany, 2012. A Preliminary Reconnaissance Report on August 11th, 2012, Varzaghan–Ahar Twin Earthquakes in NW of Iran. Report of International Association of Seismology and Physics of the Earth's Interior.

Sato, H., M.C. Fehler and T. Maeda, 2012. Seismic Wave Propagation and Scattering in the Heterogeneous Earth. Second Ed., Springer, New York, New York. 1 - 496.

Sharma, M.L. and H.R. Wason, 1994. Occurrence of low stress drop earthquakes in the Garhwal Himalaya region. Phys. Earth Planet. Int., **34**: 159 - 172.

Sharma, B., K.A. Gupta, K.D. Devi, D. Kumar, S.S. Teotia and B.K. Rastogi, 2008. Attenuation of high-frequency seismic waves in Kachch Region, Gujarat, India. Bull. seism. Soc. Am., **98**(**5**): 2325 - 2340.

Sharma J., S. Chopra and K.S. Roy, 2014. Estimation of source parameters, quality factor (Q_S), and site characteristics using accelerograms: Uttarakhand Himalaya Region. Bull. seismol. Soc. Am., **104**(**1**): 360 - 380.

Singh, S.K., A. Iglesias, R.S. Dattatrayam, B.K. Bansal, S.S. Rai, X. Perez-Campos, G. Suresh, P.R. Baidya and J.L. Gautam, 2006. Muzaffarabad Earthquake of 8 October 2005 (7.6 *Mw*): a preliminary report on source

characteristics and recorded ground motions. Current Science, **91**: 689 - 695.

Solaymani-Azad, S., S. Dominguez, H. Philip, K. Hessami, M.R. Forutan, M. Shahpasan Zadeh and J.F. Ritz, 2011. The Zandjan fault system: morphological and tectonic evidences of a new active fault network in the NW of Iran. Tectonophysics, **506**: 73 - 85.

Toksöz, M.N., D.H. Johnston and A. Timur, 1979. Attenuation of seismic waves in dry and saturated rocks-I. Laboratory Measurements. Geophysics, **44**: 681 - 690.

Zafarani, H., M. Rahimi, A. Noorzad, B. Hassani and B. Khazaei, 2015. Stochastic simulation of strong motion records from the 2012 Ahar–Varzaghan Dual Earthquakes, Northwest of Iran. Bull. Seismol. Soc. Am., **105**: 1419 - 1434.

Xu, Z. and S.Y. Schwartz, 1993. Large earthquake doublets and fault plane heterogeneity in the northern Solomon Islands subduction zone. Pure and Applied Geophysics, **140**: 365 - 390.